From Materials Development to their Test in IFMIF: an Overview

N. Baluc, R. Schäublin, P. Spätig, J. Theile, M.Q. Tran

Ecole Polytechnique Fédérale de Lausanne (EPFL), Centre de Recherches en Physique des Plasmas, Association Euratom-Confédération Suisse, Switzerland

E-mail contact of main author: nadine.baluc@psi.ch

Abstract. R&D activities on fusion reactor materials in Switzerland focus on (1) the development of advanced metallic materials for structural applications in plasma facing (first wall, divertor) and breeding blanket components of the future fusion power reactors, in particular oxide dispersion strengthened reduced activation ferritic steels and tungsten-base materials, (2) the modelling of radiation damage and radiation effects, and (3) small specimen test technology for the future International Fusion Materials Irradiation Facility. The main objectives, examples of recent results and future activities are described in the case of these three R&D areas.

1. Introduction

R&D activities on fusion reactor materials in Switzerland focus on (1) the development of advanced metallic materials for structural applications in plasma facing (first wall, divertor) and breeding blanket components of the future fusion power reactors, in particular oxide dispersion strengthened (ODS) reduced activation ferritic (RAF) steels and tungsten-base materials, (2) the modelling of radiation damage and radiation effects, and (3) small specimen test technology for the future International Fusion Materials Irradiation Facility (IFMIF). The scientific approach being used is based on investigating the structure/mechanics relationships at different length scales (nano-, micro-, meso-, and macroscopic), before and after irradiation, by using a wide range of experimental and numerical tools. For simulating experimentally the effects of 14 MeV neutrons, irradiations are being performed with a mixed spectrum of high-energy protons and spallation neutrons in the Swiss Spallation Neutron Source (SINQ) located at the Paul Scherrer Institute (PSI), Switzerland, as well as with ions in the Joint Accelerators for Nano-science and Nuclear Simulation (JANNuS) located at Orsay, France, and with fission neutrons in reactors in Belgium, Hungary and the Netherlands. The main objectives, examples of recent results and future activities are described just below in the case of the three R&D areas mentioned just above.

2. Status of R&D Activities in Switzerland

2.1. Development of Advanced Metallic Materials

The upper temperature for use of reduced activation ferritic/martensitic steels (RAFM) steels, destined to structural applications in fusion power reactors, is presently limited by a drop in mechanical strength at about 823 K [1]. ODS RAFM steels and ODS RAF steels appear promising structural materials for use up to about 923 K [1] and 1023 K [2], respectively. However, processing of ODS steels by hot isostatic pressing (HIPping) usually leads to materials with isotropic mechanical properties but relatively poor fracture properties [3], while processing by hot extrusion usually leads to materials with superior fracture properties [2] but with non-isotropic mechanical properties.

Pure tungsten exhibits high strength at high temperatures, a good surface heat capability, a good resistance to erosion, and does not suffer from high activation under neutron irradiation [4]. However, pure tungsten also shows low fracture toughness at all temperatures [5], associated with a high ductile-to-brittle transition temperature (DBTT) [6], which is strongly dependent on the chemical composition and the production history, i.e., the microstructural state. Therefore, it is usually considered that pure tungsten is well suited for plasma-facing applications, while the development of tungsten-base materials for high-temperature structural applications is still at its very beginning.

In Switzerland present activities aim at developing ODS RAF steels and reduced activation tungsten-base materials with good tensile and creep strength and sufficient ductility, especially in terms of fracture toughness and DBTT, on the basis of the following ideas (Fig. 1): (1) Alloys (e.g. W-V, W-Ti, W-Ta compounds) and nano-grained materials are expected to show an improved ductility with respect to e.g. pure tungsten and normal grain-sized materials, respectively. (2) Nano-grained materials and materials reinforced with either oxide or carbide particles are expected to show improved tensile and creep strength and radiation resistance, as (i) the particles should act as obstacles for the propagation of mobile dislocations, (ii) the numerous grain boundaries and interfaces between the matrix and the particles should act as sinks for the irradiation-induced defects, and (iii) the particles should also help stabilizing the numerous grain boundaries upon thermal annealing and/or irradiation.

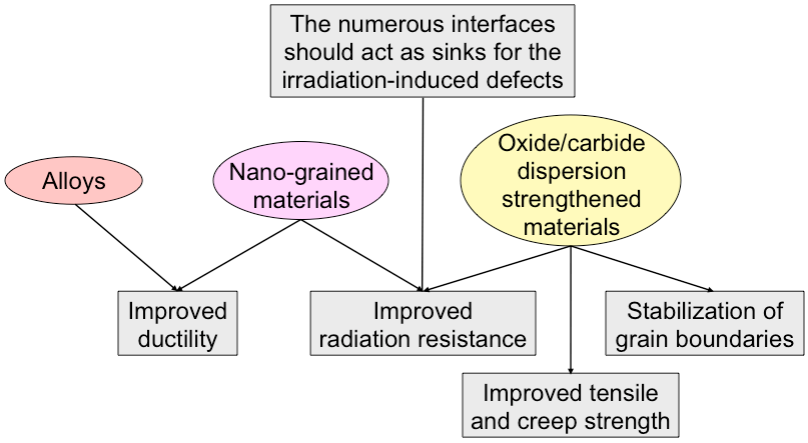

FIG. 1: Development path of ODS RAF steels and reduced activation tungsten-base materials.

ODS RAF steels: A variety of ODS RAF steels, namely Fe-(12-14)Cr-2W-(0.1-0.3-0.5)Ti-0.3Y_2O_3 (in wt.%) have been successfully produced by mechanically alloying either elemental Fe, Cr, W and Ti powders or a pre-alloyed Fe-Cr-W-Ti powder with 0.3 wt.% Y_2O_3 powder particles in a planetary ball mill, followed by compaction of the milled powders by HIPping. Detailed processing conditions are reported in e.g. [3]. It was found in particular that (1) hydrogen should be used as mechanical alloying atmosphere, in order to limit the oxygen content in the milled powders, (2) 14Cr materials exhibit a more stable ferritic microstructure than 12Cr materials, and (3) 0.5Ti materials contain large TiO_2 particles that can yield embrittlement effects. Therefore, recent R&D activities focused on the Fe-14Cr-2W-0.3Ti-0.3Y_2O_3 ODS RAF steel. When prepared using elemental powders, this material was observed to contain a bimodal distribution of coarse grains, a few micrometers in size, and smaller grains, about 200 nm in size, as well as nano-sized particles enriched with Y, Ti and O. The material exhibits high strength and reasonable elongation in tensile tests up to about 1023 K. However, it also shows relatively weak Charpy impact properties characterized by an upper shelf energy of about 3.2 J and a DBTT of about 293 K. Fortunately, the Charpy impact behaviour of ODS RAF steels can be significantly improved by the use of thermo-mechanical treatments, such as hot pressing or hot rolling [3], and/or the use of Fe_2Y particles, instead of Y_2O_3 particles, during the mechanical alloying process.

Tungsten-base materials: A variety of tungsten-base materials, namely W-(0.3-1.0-2.0)Y, W-(0-3-1.0-2.0)Y_2O_3 and W-(0.3-0.9-1.7)TiC (in wt.%) have been successfully produced by mechanically alloying a W powder with either Y or Y_2O_3 or TiC powder particles in a planetary ball mill, in an argon atmosphere, followed by either cold pressing and sintering or HIPping. Detailed processing conditions are reported in e.g. [7]. The density and microhardness of the materials were found to increase with the Y, Y_2O_3 or TiC content. Following processing by sintering a maximum density of only about 88% was measured. Much higher density values in the range of 95-97% were achieved by compacting the materials by HIPping instead of sintering. Therefore, recent activities focused on the W-2Ymaterial produced by mechanical alloying and HIPping. It was observed that the

microstructure of this material is composed of a bimodal distribution of small grains with mean sizes around 50 nm and 150 nm. The material also contains an inhomogeneous distribution of Y_2O_3 particles, with a mean size ranging between 2 to 20 nm. It seems that all yttrium transformed into yttria during manufacturing. Charpy impact tests and three-point bend tests revealed that the material is brittle up to at least 1273 K. The bending stress was observed to decrease with increasing the test temperature, from about 900 MPa at 773 K down to about 500 MPa at 1373 K. Very low fracture toughness values of about 6 MPa.$m^{1/2}$ were measured between room temperature and the maximum investigated temperature of 1273 K. Tensile tests confirmed that the material is brittle at 1273 K but ductile at 1573 K, indicating that the DBTT should lie between about 1370 K and 1470 K. Therefore, in spite of the small size of the grains, the material appears very brittle at low to moderate temperatures. As the properties of tungsten-base materials are strongly dependent on the final production step, complex thermo-mechanical treatments are being developed in the aim to improve the fracture properties of these materials.

2.2. Modelling of Radiation Damage and Radiation Effects

The main objective is to model and simulate the effects of irradiation-induced defects on (1) the microstructure and (2) the mechanical properties of pure iron and iron-base model alloys, as representative materials for RAFM steels (e.g. EUROFER 97), and of pure tungsten, as representative element for tungsten-base materials. The multiscale approach applied is based on various modelling methods, namely ab initio calculations, molecular dynamics (MD) based on the embedded atom method (EAM), and dislocation dynamics (DD) methods, allowing to span over scales. It is a multiscale inasmuch as it is based on passing information or parameters and connecting key mechanisms, through space and time scales, from the electronic/atomic (ab-initio) scale up to the structural element length and from femtoseconds up to more than seconds (DD method). Modelling results are at present being validated using the JANNuS facility by means of experimental dual and triple ion beam irradiations of ultra high purity iron-base materials.

Regarding the microstructural features of irradiated iron, starting at the lowest space scale, the self-interstitial atom (SIA) was scrutinized to identify the dependence of its formation energy, E_f^{SIA}, on temperature using ab initio calculations [8] in view of providing data for the design of a better Fe-Fe interatomic potential for MD simulations. Note that iron is the only body centred cubic (bcc) metal that accommodates a low energy <110> structure for the SIA, all others containing <111> SIAs. An unusually strong dependence of E_f^{SIA} on the entropy was found, which actually allowed solving the dilemna raised in the 80's on the structure of the SIA. The structure of a nanometric helium bubble in iron was critically investigated using MD simulations. It appears that helium has a tendency to spontaneous agglomeration with the generation of vacancies, leading to the formation of a helium bubble that is surprisingly stable, even at high pressures [9]. The resulting binding energies between helium atoms, vacancies, and SIAs, depend on the chosen empirical interatomic potentials, but show a good correspondence to ab initio results [9]. At low and moderate pressures, the helium bubble adopts a shape close to a sphere with a radius obeying a classical equation of state that depends on the internal pressure and the free surface energy of iron [10]. At high pressures the bubble surface breaks and its shape depends then on the mechanical properties of iron, with an expansion of the bubble in the soft <110> directions, giving rise to a polyhedron [10]. MD simulations showed that the presence of helium in iron has a strong influence on the damage produced by atomic displacement cascades [11,12], in promoting the formation of large SIA clusters (Fig. 2, left). The resulting damage, however, depends again strongly on the chosen empirical interatomic potentials [12], in particular on the Fe-He interaction, and at present experimental validation of this choice is still lacking.

The microstructural features of irradiated tungsten were investigated using MD simulations. With the two available interatomic potentials the lowest energy SIA in bcc tungsten appears to have a <111> structure [13]. Nanometric loops formed by SIAs platelets were investigated as a function of their size to find the lowest energy configuration. A strong dependency on the interatomic potential describing the W-W interaction was found. For one of the potential the

lowest formation energy is achieved with the ½ a_o <111>{111} loop, while in the case of the other potential the ½ a_o <111>{111} loop for radii smaller than $2a_o$ (0.63 nm, or about 20 SIAs) and the a_o <100>{100} loop for larger sizes are favourable [13], which is in contradiction with experimental observations, though scarce. MD simulations of 10, 20 and 50 keV collision cascades at 10 and 523 K in pure tungsten were performed to assess the primary damage due to irradiation, with the dependency on the interatomic potential [14]. A new approach for connecting any general EAM potential to the universal potential was developed. The three investigated potentials were observed to produce similar results, even though their displacement thresholds are quite different [14].

Dislocation lines of the screw and edge types, dislocation loops, voids, helium bubbles and chromium precipitates in iron have been successfully modelled using MD simulations, in view of simulating their impact on the propagation of mobile dislocations. It appears that these nano-sized defects act as strong obstacles to the propagation of mobile dislocations, the strongest being the voids, then the helium bubbles (Fig. 2, middle) [15,16,17], and the weakest the chromium precipitates [18]. It should be noted that a strong dependence on the choice of the interatomic potential describing the Fe-Fe interaction was found [19], despite recent efforts in potential design to match as closely as possible the elastic constants of iron, the formation energies of point defects and the magnetic behaviour of iron. The MD results were used for DD simulations, showing that the presence of a high density of nano-sized defects (Fig. 2, right) yields a strong radiation hardening [20], as measured experimentally in tensile tests. Concerning pure tungsten, the screw dislocation was investigated [21], in order to select the most appropriate potential to conduct simulations of the dislocation-defect interactions. At this point in time, the various tested potentials do not allow for a proper description of the screw dislocation core in pure tungsten [21].

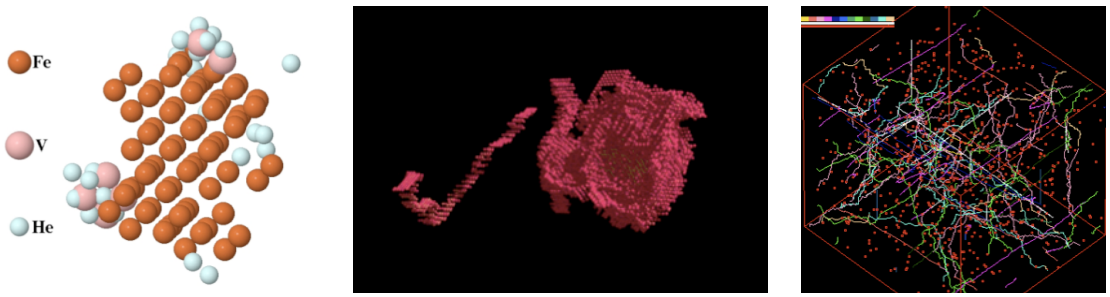

FIG. 2: (Left) MD simulation of the structure of a large SIA cluster produced by a 20 keV atomic displacement cascade at 300 K in iron containing 1.0 at.% helium interstitial atoms (v = vacancy), (middle) MD simulation of the interaction of a mobile edge dislocation with a pressurized 4 nm helium bubble at 10 K in iron under imposed strain rate, promoting strong loop punching, and (right) DD simulation of the effect of 10^{22} m^{-3} 2 nm voids on 10^{12} m^{-2} mobile dislocations at 300 K in iron, yielding a strong radiation hardening in tensile tests.

In order to provide experimental validation, transmission electron microscopy (TEM) appears the most suitable method as it provides direct imaging of the simulated defect structures. TEM image simulations were undertaken in order to close the gap between the modelling and the experimental observations, and to study the condition of visibility of the nanometric defects that are usually at the spatial resolution limits of the TEM [22].

2.3. Small Specimen Test Technology

Small specimen test techniques: The main reason to develop and make use of small specimen test techniques is driven by the rather limited irradiation volume in current and future irradiation facilities. Fracture toughness is particularly sensitive to the specimen size and geometry. Therefore, adequate methods to account for the specimen size and geometry effects on the fracture toughness have to be developed. Neutron irradiations are always detrimental for the fracture properties of RAFM and ODS RAFM steels, whose crystalline structure is bcc [23]. It is well known that the metals and alloys with a bcc structure exhibit a ductile-to-brittle transition of the fracture mode by decreasing the temperature. One major

effect of neutron irradiation is to shift the transition region to higher temperatures; this phenomenon is called embrittlement. The amplitude of the temperature shift depends on the irradiation conditions: temperature, neutron flux and fluence, amounts of He and H produced by nuclear transmutation reactions, and so on. The method of the master-curve, based on the determination of the reference temperature T_o that indexes a median universal toughness-temperature curve at 100 MPa.m$^{1/2}$, appears as a powerful method to determine the temperature shift with a limited number of specimens [23]. From very large databases on reactor-pressure vessel (RPV) steels, it was established that the universal median toughness-temperature curve reads as [24]:

$$K_{med} = 30 + 70 \exp(0.019(T-T_o)) \quad (1)$$

and holds for toughness data obtained from 1T-thick compact tension (C(T)) specimens (1T = 25.4 mm). In addition, the master-curve provides a statistical tool to describe the scatter of the toughness data at a given temperature through a three-parameters cumulative Weibull distribution function [25]. While having been initially developed for tempered bainitic RPV steels, the master-curve method was shown to describe the entire F82H-mod RAFM steel fracture database rather satisfactorily [26], provided that the specimen size effects are taken into account. Results of fracture toughness tests performed on F82H-mod specimens irradiated in the High Flux Reactor (HFR) at Petten, the Netherlands, in two irradiation conditions, namely at 333 K to 2.2 dpa and at 573 K to 2.1 dpa, are reported in [27]. The data were obtained with sub-sized C(T) specimens and the toughness behaviour in the transition is shown in Fig. 3 (left), where both unirradiated and irradiated data (irradiation at 573 K to 2.1 dpa) are plotted to illustrate the temperature shift, ΔT_o, of the toughness-temperature curve. Since ΔT_o stems from the concomitant radiation hardening, defined as the increase in yield stress after irradiation, $\Delta\sigma_y$, a comparison of the temperature shifts for different irradiation conditions must take into account the corresponding radiation hardening values. A simple but reasonable approach is to consider a linear relation between ΔT_o and $\Delta\sigma_y$. Such an analysis for the F82H-mod RAFM steel was done by Yamamoto et al. [28] who found: $\Delta T_o = \alpha\, \Delta\sigma_y$ with $\alpha = 0.58$. While some refinements have already been proposed to better take into account the overall effects of irradiation on the plastic flow by calculating an average flow stress increase instead of $\Delta\sigma_y$ [29], we emphasize that good predictions of embrittlement can be derived simply from the measure of the radiation hardening. It was also shown that the ΔT_o shifts of the EUROFER 97 RAFM steel can be determined with ultra-small specimens [30]. Indeed, three-points bend bars of 1x1x12 mm^3 were tested before and after irradiation at 573 K to 0.5 dpa in a 590 MeV proton beam at the PSI. The $\Delta T_o/\Delta\sigma_y$ value obtained using these ultra-small specimens is 0.53, which is quite consistent with the average value obtained for the F82H-mod RAFM steel (see above). Note that the ΔT_o shifts were determined from the fits to the data below 100 MPa.m$^{1/2}$ to avoid the excessive constraint loss occurring in the upper transition region.

As mentioned above, the master-curve methodology was initially developed for RPV steels. Some authors raised questions and concerns regarding the applicability of the master-curve to RAFM steels [31]. In particular, it was not clear whether the amplitude of the scatter of the toughness data in the transition region can be described by the RPV master-curve approach properly. Indeed, in the case of the F82H-mod RAFM steel, the data assembled by Odette et al. [26] revealed an excessive scatter with respect to the theoretical predictions of the master-curve. In order to assess the applicability of the master-curve to RAFM steels, a large number of fracture tests on the EUROFER 97 RAFM steel were undertaken [32]. The testing matrix included thick C(T) specimens, namely 0.87T C(T), as well as sub-sized 0.18T and 0.36T C(T) ones. Enough data were obtained to fit not only T_o of equation (1) but also a second parameter to allow for an adjustment of the master-curve shape. In order to keep the meaning of T_o as the reference temperature at which the median toughness is 100 MPa.m$^{1/2}$, two parameters were fitted: A and T_o of the equation $K_{med} = A + (100\text{-}A) \exp(0.019(T\text{-}T_o))$. The parameters were deduced from the method of the maximum likelihood and it was found that, for EUROFER 97, the data are very well described by a master-curve of equation:

$$K_{med} = 12 + 88 \exp(0.019(T-T_o)) \quad (2)$$

The toughness data versus temperature are plotted in Fig. 3 (right) along with the master-curve, the 1% and 99% failure bonds, and the prediction of the model (see below). While being modest, the difference between equations (1) and (2) has all its importance when the testing is focused, or must be focused, in the lower transition region near the lower shelf. The major point to underscore here is that the specimen size effect on the measured fracture toughness, for a given size, decreases with the value of the toughness. In other words, it is highly desirable to test the small specimens in the lower part of the transition region. Thus, with the typical sub-sized facture specimens foreseen to be irradiated in IFMIF, it is of primary importance to have a good description of the master-curve in the lower part of the transition and not to overlook the importance of the master-curve shape adjustments to determine T_o accurately. More details highlighting that point can be found in [32].

Finally, it is important to mention that modelling of the fracture behaviour is a necessary step to transfer the data from one specimen size to another. The red dots in Fig. 3 (right) refer to predictions based upon a local approach of fracture, where it is assumed that the onset of fracture is controlled by a critical stress/strain state at the crack tip. The simplest criterion of brittle fracture used to reconstruct the 1% failure bond in Fig. 3 (right) relies on the attainment of a critical maximum principal stress value (σ^*) over a critical volume (V^*) or area (A^*) [23]. This criterion is illustrated in Fig. 3 (right) where an iso-stress contour around a crack tip is drawn. The procedure to calibrate the criterion σ^*-A^* is described in details in [33], and the practical application to transfer data from one specimen size to another is given in [34].

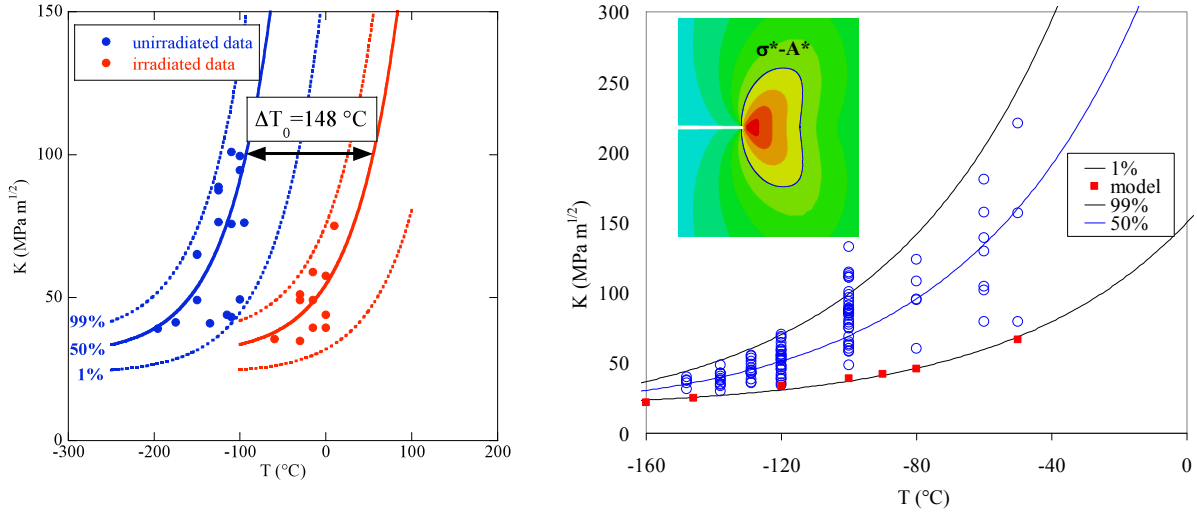

FIG. 3: (Left) Shift of the toughness-temperature curve of the F82H-mod RAFM steel after neutron irradiation at 573 K to 2.1 dpa, measured with 0.18T C(T) specimens, and (right) description of the EUROFER 97 fracture toughness versus temperature with the master-curve of equation (2) and model. The insert shows an iso-stress contour around a loaded crack: σ^*-A^* is the local criterion for fracture of the model.

Design of a creep-fatigue test module for IFMIF: A test module for performing in-situ creep-fatigue tests, under intense neutron irradiation, in the medium flux test module of IFMIF [35] has been conceived and designed (Fig. 4). This module is referred to as the creep-fatigue test module (CFTM) and will allow creep-fatigue testing of three specimens independently. The information obtained in these experiments will be of special relevance for structural materials to be used in DEMO-type reactors and beyond.

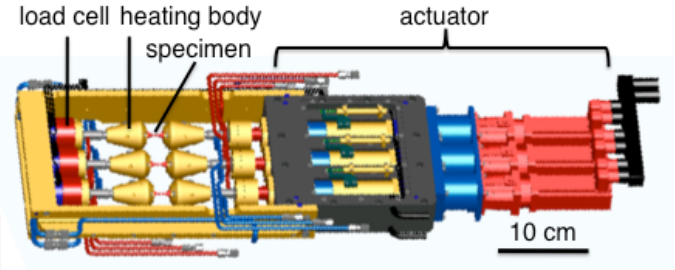

FIG. 4: Schematics of the CFTM for IFMIF.

3. Acknowledgements

The Paul Scherrer Institute is acknowledged for the overall use of its facilities. This work, supported by the European Communities under the contract of Association between EURATOM/Confédération Suisse, was carried out within the framework of the European Fusion Development Agreement. The views and opinions expressed herein do not necessarily reflect those of the European Commission. This work was also performed within the framework of the Integrated European Project „ExtreMat“ (contract NMP-CT-2004-500253) with financial support by the European Community. It only reflects the view of the authors and the European Community is not liable for any use of the information contained therein. Part of this work was supported by the Swiss Voluntary Contribution to the Broader Approach Agreement between Euratom and JAEA.

4. References

[1] LINDAU, R., et al., ‘Present development status of EUROFER and ODS-EUROFER for application in blanket concepts’, Fusion Engineering and Design **75–79** (2005) 989–996.
[2] McCLINTOCK, D.A., et al., ‘Mechanical properties of irradiated ODS-EUROFER and nanocluster strengthened 14YWT’, Journal of Nuclear Materials **392** (2009) 353-359.
[3] OKSIUTA, Z., BALUC, N., ‘Optimization of the chemical composition and manufacturing route for ODS RAF steels for fusion reactor application’, Nuclear Fusion **49** (2009) 055003 (8pp).
[4] BALUC, N., ‘Assessment report on tungsten’, Final Report on the EFDA Task TW1-TTMA-002 Deliverable 5, (2002).
[5] ZINKLE, S.J., GHONIEM, N.M., ‘Operating temperature windows for fusion reactor structural materials’, Fusion Engineering and Design **51-52** (2000) 55-71.
[6] RIETH, M., DAFFERNE, B., ‘Limitations of W and W–1%La2O3 for use as structural materials’, Journal of Nuclear Materials **342** (2005) 20-25.
[7] VELEVA, L., et al., ‘Sintering and characterization of W-Y and W-Y2O3 materials’, Fusion Engineering and Design **84** (2009) 1920-1924.
[8] LUCAS, G., SCHAUBLIN, R., ‘Vibrational contributions to the stability of point defects in bcc iron: A first-principles study’, Nuclear Instruments & Methods in Physics Research Section B-Beam Interactions with Materials and Atoms **267** (2009) 3009-3012.
[9] LUCAS, G., SCHAUBLIN, R., ‘Stability of helium bubbles in alpha-iron: A molecular dynamics study’, Journal of Nuclear Materials **386** (2009) 360-362.
[10] HAGHIGHAT, S.M.H., et al., ‘State of a pressurized helium bubble in iron’, Europhysics Letters **85** (2009) 60008 (5pp).
[11] YU, J.N. et al, ‘Synergistic effects of PKA and helium on primary damage formation in Fe-0.1%He’, Journal of Nuclear Materials **367** (2007) 462-467.
[12] LUCAS, G., SCHAUBLIN, R., ‘Helium effects on displacement cascades in alpha-iron’, Journal of Physics-Condensed Matter **20** (2008) 415206 (12pp).
[13] FIKAR, J., SCHAUBLIN, R., ‘Atomistic simulations of nanometric dislocation loops in bcc tungsten’, Nuclear Instruments & Methods in Physics Research Section B-Beam Interactions with Materials and Atoms **267** (2009) 3218-3222.
[14] FIKAR, J., SCHAUBLIN, R., ‘Molecular dynamics simulation of radiation damage in bcc tungsten’, Journal of Nuclear Materials **386** (2009) 97-101.
[15] SCHAUBLIN, R., CHIU, Y.L., ‘Effect of helium on irradiation-induced hardening of iron: A simulation point of view’, Journal of Nuclear Materials **362** (2007) 152-160.

[16] HAFEZ HAGHIGHAT, S.M., SCHAUBLIN, R., 'Molecular dynamics modeling of cavity strengthening in irradiated iron', Scientific Modeling and Simulation **14** (2007) 191-201.
[17] HAGHIGHAT, S.M.H., SCHAUBLIN, R., 'Influence of the stress field due to pressurized nanometric He bubbles on the mobility of an edge dislocation in iron,' Philosophical Magazine **90** (2010) 1075-1100.
[18] TERENTYEV, D., et al., 'Strengthening due to Cr-rich precipitates in Fe-Cr alloys: Effect of temperature and precipitate composition', Journal of Applied Physics **107** (2010) 061806 (8pp).
[19] HAGHIGHAT, S.M.H., et al., 'Effect of interatomic potential on the behavior of dislocation-defect interaction simulation in alpha-Fe', Journal of Nuclear Materials **382** (2008) 147-153.
[20] HAGHIGHAT, S.M., 'Multiscale modelling of irradiation induced effects on the plasticity of Fe and Fe-Cr', EPFL PhD thesis No. 4667 (2010).
[21] FIKAR, J., et al., 'Atomistic simulation of 1/2 < 111 > screw dislocations in BCC tungsten', 1st International Conference on New Materials for Extreme Environments **59** (2009) 247-252.
[22] SCHAUBLIN, R., 'Nanometric crystal defects in transmission electron microscopy', Microscopy Research and Technique **69** (2006) 305-316.
[23] ODETTE, G.R., et al., 'Cleavage fracture and irradiation embrittlement: mechanisms, toughness measurements and implications to structural integrity assessment', Journal of Nuclear Materials **323** (2003) 313-340.
[24] WALLIN, K., 'Irradiation damage effects on the fracture toughness transition curve shape for reactor pressure vessel steels', International Journal of Pressure Vessels and Piping **55** (1993) 61-79.
[25] WALLIN, K., 'Macroscopic nature of brittle fracture', Journal de Physique IV **3** (1993) 575-584.
[26] ODETTE, G.R., et al., 'A master curve analysis of F82H using statistical and constraint loss size adjustments of small specimen data', Journal of Nuclear Materials **329-333** (2004) 1243-1247.
[27] SPÄTIG, P., et al., 'Plastic flow properties and fracture toughness characterization in the low transition of unirradiated and irradiated tempered martensitic steels', Journal of Nuclear Materials **367-370** (2007) 527-538.
[28] YAMAMOTO, T., et al., 'Evaluation of fracture toughness master curve shifts for JMTR irradiated F82H using small specimens', Journal of Nuclear Materials **367-370** (2007) 593-598.
[29] ODETTE, G.R., 'On the relation between irradiation induced changes in the master curve reference temperature shift and changes in strain hardened flow stress', Journal of Nuclear Materials **367-370** (2007) 561-567.
[30] SPÄTIG, P., et al., 'Assessment of irradiation embrittlement of the Eurofer97 steel after 590 MeV proton irradiation', Journal of Nuclear Materials **386-388** (2009) 245-248.
[31] LUCON, E., 'A closer look at the fracture toughness of ferritic/martensitic steels', Journal of Nuclear Materials **367-370** (2007) 575-580.
[32] MUELLER, P., 'Fracture toughness master-curve analysis of the tempered martensitic steel Eurofer97', Journal of Nuclear Materials **386-388** (2009) 323-327.
[33] BONADE, R., et al., 'Fracture toughness behavior in the ductile-brittle transition region of the tempered martensitic Eurofer97 steel: Experiments and modeling', Engineering Fracture Mechanics **75** (2008) 3985-4000.
[34] MUELLER, P., SPÄTIG, P., '3D finite element and experimental study of the size requirements for measuring toughness on tempered martensitic steels', Journal of Nuclear Materials **389** (2009) 374-384.
[35] IFMIF INTERNATIONAL TEAM, 'IFMIF Comprehensive Design Report', (2003).